Volume 2
Number 6
June 2024
Pages 1623–1896

RSC Sustainability

rsc.li/rscsus

ISSN 2753-8125

ROYAL SOCIETY OF CHEMISTRY

PAPER
Patritsia M. Stathatou, Patrick S. Doyle *et al.*
Yeast-laden hydrogel capsules for scalable trace lead removal from water

RSC Sustainability

ROYAL SOCIETY OF CHEMISTRY

PAPER

View Article Online
View Journal | View Issue

Check for updates

Cite this: *RSC Sustainability*, 2024, **2**, 1761

Yeast-laden hydrogel capsules for scalable trace lead removal from water†

Devashish Gokhale,‡[a] Patritsia M. Stathatou,‡*[bc] Christos E. Athanasiou[d] and Patrick S. Doyle *[ae]

Trace heavy metals are present in water resources globally, jeopardizing ecosystems and human health. Lead is one of the most prevalent and toxic trace pollutants, with numerous incidents of lead-contaminated drinking water across the United States. Conventional treatment processes fail to remove trace lead from water in a resource-efficient manner. Yeast can effectively remove lead from water *via* a rapid mass transport process, called biosorption, even when lead concentrations are below 1 part-per-million. Rapid and high lead uptake can enable the application of this inexpensive and abundant biomaterial to water treatment, but scalability is limited by the need to remove any added yeast from water. Here, we scale up a yeast-based treatment process without requiring additional separation steps. Yeast cells are confined within hydrogel capsules that are sufficiently large for easy separation from water by gravitational settling, and sufficiently porous not to limit adsorption capacity and kinetics. The yeast-laden capsules exhibit an uptake capacity of 21 mg g^{-1}, comparable to free yeast under the same conditions, reaching equilibrium within the first 5 minutes of contact. We assess the mechanical robustness of the yeast-laden capsules, and construct a lab-scale proof-of-concept packed-bed biofilter, capable of treating trace lead-contaminated water and meeting USEPA drinking water guidelines while operating continuously for 12 days, to demonstrate the scalability of our approach. By overcoming common separation and structural stability issues that limit scalability of biological water treatment methods, our work offers an innovative and sustainable solution targeting emerging contaminants.

Received 2nd February 2024
Accepted 2nd April 2024

DOI: 10.1039/d4su00052h

rsc.li/rscsus

Open Access Article. Published on 15 May 2024. Downloaded on 2/18/2026 8:24:31 AM.
This article is licensed under a Creative Commons Attribution-NonCommercial 3.0 Unported Licence.

Sustainability spotlight

Lead is highly toxic even at trace concentrations, posing a significant health threat despite regulations. Conventional treatment processes are expensive, unsustainable, and resource inefficient. Low-cost yeast-based solutions are promising alternatives but are hindered by the need for additional separation to remove yeast from water. We address this limitation by encapsulating yeast cells in hydrogel capsules made in facile, scalable processes, and use the capsules to create affordable, long-lasting, flow-through filters that treat contaminated water to drinking water standards. Careful hydrogel design ensures effective yeast retention without compromising lead adsorption capacity, mechanical robustness, and removal kinetics. This strategy, applicable to diverse water treatment methods, offers an environmentally friendly, transformative approach to water quality enhancement with broad implications for global health.

1 Introduction

Removing heavy metals and particularly lead from water resources is an issue of utmost importance for public health and ecosystem preservation.[1–5] A recent study[6] underscores the gravity of this concern, revealing an annual toll of over 400 000 fatalities due to lead poisoning in the United States alone, a figure exceeding by sevenfold the mortality attributed to influenza each year.[7] It is highly likely that a substantial majority of these incidents are linked to the consumption of lead-contaminated drinking water and it is estimated that approximately 20% of these lead-related fatalities could have been prevented by improved water treatment.[6,8] Lead can enter drinking water through inadequate water treatment or due to chemical reactions with lead-containing components of water

[a]*Department of Chemical Engineering, Massachusetts Institute of Technology, Cambridge, MA 02139, USA. E-mail: pdoyle@mit.edu*

[b]*Renewable Bioproducts Institute, Georgia Institute of Technology, Atlanta, GA 30332, USA. E-mail: patricia@gatech.edu*

[c]*Center for Bits and Atoms, Massachusetts Institute of Technology, Cambridge, MA 02139, USA*

[d]*Daniel Guggenheim School of Aerospace Engineering, Georgia Institute of Technology, Atlanta, GA 30332, USA*

[e]*Harvard Medical School Initiative for RNA Medicine, Boston, MA 02215, USA*

† Electronic supplementary information (ESI) available. See DOI: https://doi.org/10.1039/d4su00052h

‡ These authors contributed equally to this work.

© 2024 The Author(s). Published by the Royal Society of Chemistry

Open Access Article. Published on 15 May 2024. Downloaded on 2/18/2026 8:24:31 AM. This article is licensed under a Creative Commons Attribution-NonCommercial 3.0 Unported Licence.

distribution systems, which not only affect underserved or disadvantaged communities.[8,9] Beyond the high-profile lead-related water crises in Flint, Michigan and Washington, D.C. during the past decade, numerous lead contamination incidents have been reported in various locations across the country, including in Wisconsin, Maryland, and Chicago.[8,10]

The US Environmental Protection Agency (USEPA) established the Lead and Copper Rule in 1991 to control lead in drinking water and protect public health.[11] According to this rule the Maximum Contaminant Level Goal (MCLG) for lead is zero, since there is no safe level of lead exposure (as even trace amounts ingested over time can result in adverse effects due to bioaccumulation). This rule also established action levels for lead in drinking water as measures of the effectiveness of the corrosion control treatment in water systems. The action level for lead is 15 parts per billion (ppb), and if lead concentrations exceed this action level in more than 10% of the customer taps sampled, then several control actions must be performed including public education and lead service line replacement.[12] The rule was revised in 2021 introducing a lead trigger level of 10 ppb for proactive planning in communities with lead service lines.[13] Although the MCLG for lead in the US is zero, a study in 2021 uncovered detectable, alarming lead levels in almost all water samples collected from 120 sites across 36 US states ranging from 0.01–11.20 ppb.[14,15]

Several physicochemical water treatment methods exist for removing trace lead from drinking water at the household and community levels, with reverse osmosis (RO) filtration systems being among the most efficient ones. Nonetheless, such systems result in substantial financial and environmental costs to eliminate trace lead amounts.[16] Costs of RO systems range from around $150 for under-the-sink compact filters to $20,000 for commercial or large residential setups, without including the significant installation and maintenance expenses.[17] In parallel, RO systems generate considerable volumes of wastewater to operate, since typical point-of-use systems can generate 5–10 gallons of wastewater for every gallon of treated water produced with the more efficient units achieving a 1 : 1 rejected to clean water ratio.[17,18] They also require significant amounts of energy (~4 kW h m^{-3} of water[19]), roughly an order of magnitude higher than the average specific energy expenditure of US water and wastewater treatment facilities.[20]

Biosorption, a mass transfer process by which an ion or molecule binds onto inactive biological materials by physicochemical interactions,[21] can offer a sustainable and effective alternative to conventional processes. As shown previously,[1] trace lead can be effectively removed from water by using the yeast *Saccharomyces cerevisiae* (*S. cerevisiae*). Yeast rapidly treats water with environmentally relevant initial lead concentrations below 1 part per million (ppm), attaining equilibrium within the first 5 min of contact. Most adsorption processes in water treatment facilities have limited contact times (~10 min), making rapid removal essential.[22,23] Further, *S. cerevisiae* yeast can be acquired at minimal or even zero cost in large quantities, as a common waste product of various fermentation industries.[24–26] Surplus yeast is currently produced in huge volumes and is an extremely underutilized low-value resource not suitable as a human dietary supplement due to high levels of nucleic acids.[1,27] The large-scale application of this inexpensive and abundant biomaterial could be highly advantageous to achieve rapid and high lead uptake, while enhancing the application of circular economy models within local contexts. The main limitation in implementing such processes resides in the need for supplementary treatment stages to remove the introduced yeast from water.

In this study, this limitation is overcome through the encapsulation of yeast cells in hollow capsules made of poly(ethylene glycol) diacrylate (PEGDA) hydrogel (Fig. 1). PEGDA capsules are more stable than other hydrogels used in literature due to chemical crosslinking.[28] PEGDA is an economical and biocompatible material that has seen prior use in water treatment applications.[29] The developed hydrogel capsules serve as yeast-containing vessels, large enough to be easily separated from water under the effect of gravity or by using commercial frits that do not significantly contribute to pressure drop. Hydrogels have several inherent advantages that make them an ideal platform to encapsulate yeast cells, increasing the effective size of the cells while retaining functionality. For instance, hydrogels have seen extensive use in water treatment in prior work, and are known to rapidly sequester contaminants due to their high porosity which allows rapid mass transport.[29–31] Hence, encapsulating yeast inside hydrogels is expected not to impose significant kinetic limitations on the treatment process compared to using free yeast cells in water. Furthermore, a significant body of work in the field of bioengineering demonstrates that hydrogels can be made using chemistries compatible with yeast cells,[32,33] implying minimal function-affecting interactions between the cells and the surrounding hydrogel matrix. Therefore, it can be expected that

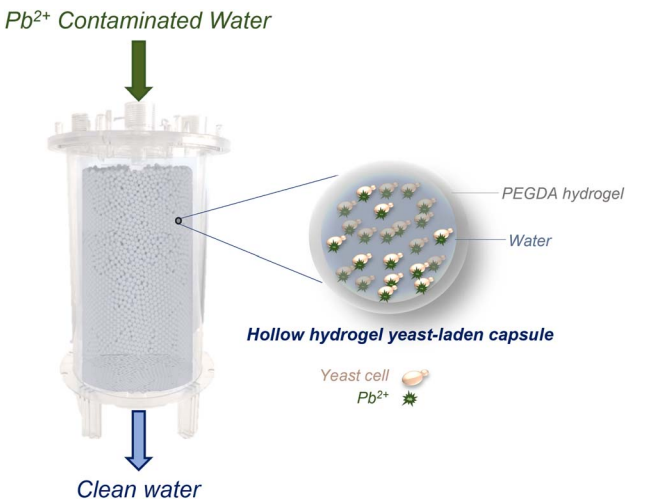

Fig. 1 Concept schematic of the developed approach for scaling up the trace-lead biosorption process. A packed-bed biofilter consisting of yeast-laden capsules: lead-contaminated water enters the biofilter and lead ions diffuse into the porous hollow hydrogel capsules, as shown in the magnified inset. Lead ions are captured by yeast cells which are freely-moving within the hollow part of the capsule. Clean water is collected at the biofilter outlet.

© 2024 The Author(s). Published by the Royal Society of Chemistry

Open Access Article. Published on 15 May 2024. Downloaded on 2/18/2026 8:24:31 AM.
This article is licensed under a Creative Commons Attribution-NonCommercial 3.0 Unported Licence.

encapsulating yeast cells within hydrogel particles will not significantly affect yeast–lead interactions.

We demonstrate the use of hydrogel beads and capsules synthesized using an off-the-shelf microfluidic device (microcross) to indefinitely encapsulate yeast and rapidly clean lead-contaminated water at environmentally relevant concentrations (ppb levels). Our results showcase that the use of hollow PEGDA hydrogel capsules offers significant advantages as a support matrix over solid hydrogel beads. A capsule-based formulation protects yeast cells from the polymerization reaction and enables their direct contact with contaminants, avoiding potential kinetics and adsorption limitations occurring from yeast–hydrogel interactions. In addition, the capsules have sufficient mechanical robustness to enable their use in a packed-bed, flow-through biofilter that serves as a proof-of-concept bioreactor illustrating the scale-up potential of the proposed approach. Previous attempts to scale-up biosorption using immobilized microbial cells have failed mostly due to chemical alterations of cell structures caused by immobilization agents, lack of mechanical robustness, and unfavorable solute mass transfer rates.[21] In contrast, our approach successfully addresses these challenges, enabling yeast to perform nearly as effectively as in its free state while encapsulated. Overall, this work overcomes separation and structural stability issues that could limit biosorption scalability and showcases the scale up of a highly effective, environmentally friendly, inexpensive, benign to human health, and easy-to-mass-produce advanced treatment process that could be applied to target emerging contaminants, enabling circular economy models.

2 Materials and methods

2.1 Glassware cleaning

Glassware was autoclaved for 15 min at 121 °C (Amsco Lab 250 sterilizer, STERIS, Ireland) and rinsed three times with Type I ultrapure water, with a resistivity of 18.2 MΩcm at 25 °C and total organic carbon (TOC) <5 ppb (Milli-Q Direct 8 Water Purification System, Millipore Sigma, USA). Phosphate-free detergent, suitable for trace heavy metals analyses, was used to wash the glassware (Liquinox detergent, Alconox, USA), which was then rinsed 3 times with ultrapure water and soaked in a 20% nitric acid (HNO_3) bath for at least 24 h. The HNO_3 bath was made using 69% HNO_3 (ARISTAR PLUS, VWR Chemicals BDH, VWR, USA) and ultrapure water. After soaking in the 20% HNO_3 bath, flasks were rinsed 3 times with ultrapure water prior to use.[1]

2.2 Yeast strain & culture

The *S. cerevisiae* Meyen ex E.C. Hansen MYA-796 strain, obtained from ATCC (USA), was utilized. YM agar and broth media (ATCC 200 YM Medium, ATCC, USA) were employed for the yeast cultures. The yeast cells were incubated in 2 L Erlenmeyer flasks containing shallow medium (200 ml) using a Gyromax 737 orbital incubator shaker (Amerex Instruments, Inc., USA) at 30 °C and 200 rpm. The protocol and processes described in Stathatou *et al.*, 2022 were followed.[1]

2.3 Biomass harvesting, washing & lyophilization

Yeast cells were harvested by centrifugation at 1000 × g for 10 min (Sorvall Legend XTR centrifuge, Thermo Fisher Scientific Inc., USA) and washed by two successive suspensions and centrifugations with ultrapure water. Harvested, washed cells were kept at −30 °C for 24 h and then inserted in the freeze dryer (Freezone 6 Liter Manifold freeze dryer, Labconco, USA).[1] Each lyophilization cycle (temperature <−40 °C, pressure <0.371 mbar) lasted for at least 50 h. Lyophilized cells (powder form) were stored in a desiccator containing silica gel. Freeze-dried biomass was weighted using an analytical balance of 0.1 mg precision and resolution.

2.4 Preparation of aqueous solutions

Type I ultrapure water was spiked with lead(II) nitrate (Sigma-Aldrich, USA) to achieve solutions with initial Pb^{2+} concentrations of up to 1000 ppb. The initial solution pH was adjusted to between 4.7 and 5.2 by using 70% nitric acid (Sigma-Aldrich, USA). The pH of aqueous solutions was measured using a glass-body electrode suitable for ion-weak samples (Orion Star A215, Thermo Scientific, USA).[1]

2.5 Capsule preparation

Yeast-containing hydrogel capsules were prepared using a scalable microfluidics setup as shown in Fig. 2a, using a protocol inspired by prior work.[34] The hydrophobic oil phase consists of 70% (v/v) dodecane, 15% (v/v) tetradecane, 10% (v/v) Span 80 (all from Sigma-Aldrich, USA), and 5% (v/v) Abil EM 90 (Evonik Industries, USA), in which the photoinitiator bis(2,4,6-trimethylbenzoyl)phenylphosphine oxide (1 mg ml^{-1}) (Sigma-Aldrich, USA) is dissolved. To obtain the aqueous monomer phase, clumps of lyophilized yeast are gently broken apart and slowly added to deionized water followed by the addition of poly(ethylene glycol) diacrylate (PEGDA, MW 700) (Sigma-Aldrich, USA) to obtain a 5% (w/v) yeast suspension in a 40% (v/v) PEGDA, 60% (v/v) deionized water base. Pluronic F127 (Sigma-Aldrich, USA) is added to this suspension (0.05% w/v) to stabilize it. Both phases are purged with argon gas for 30 min before use in the microfluidics setup.

The microfluidics setup is assembled as shown in Fig. S1†. All parts (excluding syringes) are ultrasonicated in a 1 M sodium hydroxide (NaOH) (VWR, USA) solution for 60 min and then washed with 200-proof ethanol (VWR, USA). These parts are allowed to dry in ambient conditions to remove ethanol before assembly. The cleaned and assembled parts are then filled with a 2.5% (w/v) solution of Pluronic F127 (Sigma-Aldrich, USA) for 10 min to pre-condition the setup and prevent the agglomeration of yeast cells within the microcross, before syringes filled with the oil and monomer phases are attached as shown in Fig. S1†. The syringe pumps are started and droplet formation allowed to reach equilibrium before the UV lamp is turned on, and capsules may then be collected at the outlet. The prepared capsules are washed with deionized water to remove any oil and unreacted reagents before use in experiments.

Open Access Article. Published on 15 May 2024. Downloaded on 2/18/2026 8:24:31 AM.
This article is licensed under a Creative Commons Attribution-NonCommercial 3.0 Unported Licence.

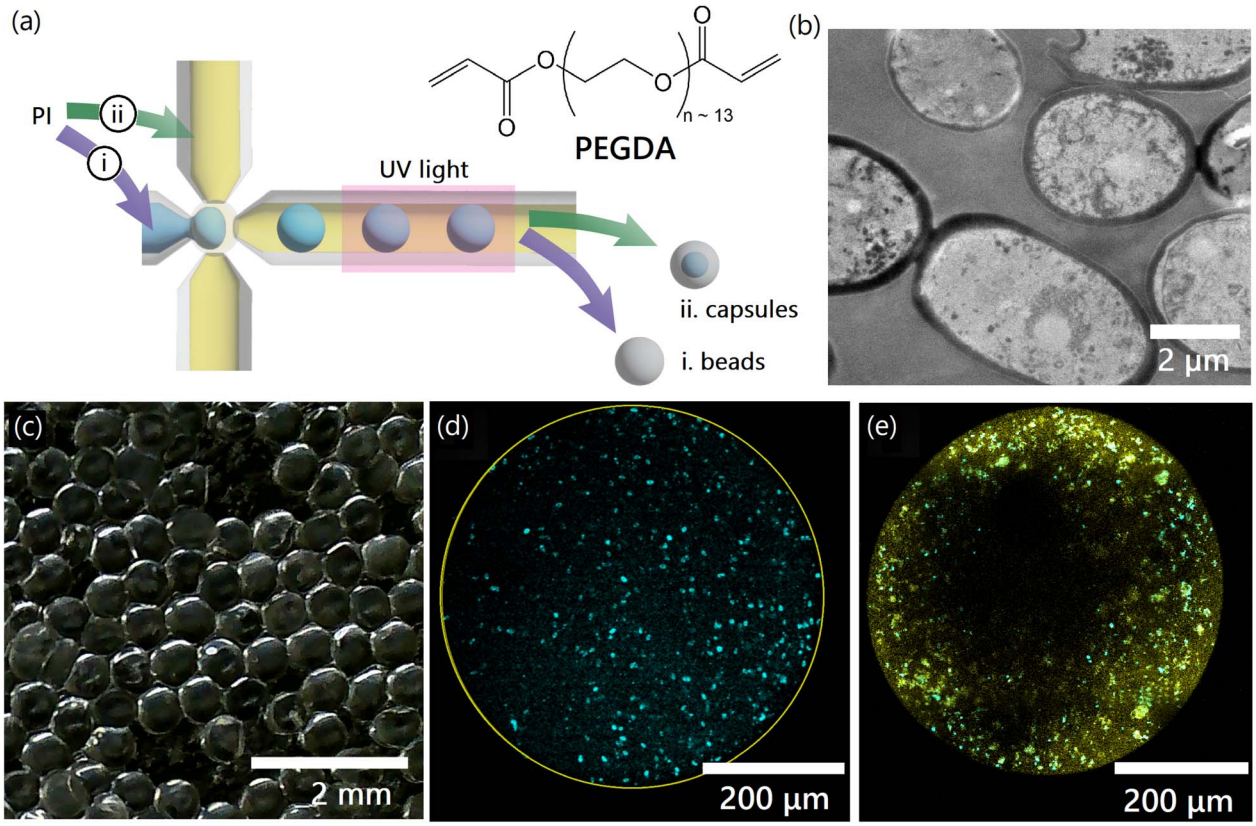

Fig. 2 Synthesis and characterization of yeast-laden hydrogels. (a) Monomer solutions are used to prepare droplets using an off-the-shelf microfluidic device with inlets on the (top), (left), and (bottom), and an outlet on the (right). Droplets are UV-polymerized into: (i). beads, or (ii). capsules, based on whether the photoinitiator (PI) is dissolved in the aqueous monomer phase (blue) or the hydrophobic oil phase (yellow). PEGDA, shown in the inset, is the hydrogel precursor in the monomer solution. (b) Scanning electron microscopy images of individual free yeast cells. (c) Hydrogel capsules containing yeast cells. (d) Confocal microscopy image showing the distribution of stained yeast cells on the central plane of unstained hydrogel bead (outer wall in yellow). (e) Confocal microscopy image showing the distribution of stained yeast cells (cyan) on the central plane of a stained hydrogel capsule (capsule walls in yellow).

2.6 Bead preparation

Solid hydrogel beads containing yeast cells are prepared using the same setup described previously, which is also assembled and operated as previously described. To obtain solid beads, a hydrophobic oil phase consisting of mineral oil (Sigma-Aldrich, USA) is used in combination with an aqueous monomer phase consisting of finely ground 5% (w/v) yeast biomass suspended in a 10% (v/v) PEGDA (Sigma-Aldrich, USA), 5% (v/v) 2-hydroxy-2-methylpropiophenone (as photoinitiator) (Sigma-Aldrich, USA) solution in deionized water. The prepared beads are washed with deionized water to remove any oil and unreacted reagents before use in experiments.

2.7 Biosorption experiments & ICP-MS

All biosorption experiments were conducted in batch contact environments using 2 L Erlenmeyer flasks with one of: lyophilized yeast cells, hydrogel beads/capsules containing yeast cells, or blank control hydrogel beads/capsules added to 200 ml of Pb^{2+} containing aqueous solutions. In all experiments using free and encapsulated yeast, the total amount of yeast added was kept constant at 5 mg (corresponding to a total bead/capsule mass of 100 mg containing 5% (w/w) encapsulated yeast). Control experiments using blank control beads/capsules were performed using the equivalent amount of hydrogel beads/capsules (95 mg). Flasks were incubated at 200 rpm and 25° (Gyromax 737 orbital incubator shaker, Amerex Instruments, Inc., USA). After the required contact time, yeast biomass was separated from the aqueous solutions by centrifugation at 2000 rpm for 10 min (Sorvall Legend XTR centrifuge, Thermo Fisher Scientific Inc., USA). The supernatants were analyzed using inductively coupled plasma mass spectrometry (ICP-MS) (7900 ICP-MS system, Agilent, USA) to measure the residual Pb^{2+} concentrations following standard operating procedures (Pb^{2+} calibration standards and Bismuth internal standard, Agilent, USA). All experiments were carried out in triplicate and mean values are reported.

For all experiments, a control sample of ultrapure water spiked with $Pb(NO_3)_2$ in absence of yeast and hydrogels was measured to act as a reference for the initial Pb^{2+} concentration, c_0, in the solution. Pb^{2+} removal was quantified by taking the ICP-MS measurements of the supernatants and subtracting from this the reference to determine the quantity of metal adsorbed by yeast biomass. Type I ultrapure water alone was also tested *via* ICP-MS to make sure that there was no Pb^{2+}

© 2024 The Author(s). Published by the Royal Society of Chemistry

Open Access Article. Published on 15 May 2024. Downloaded on 2/18/2026 8:24:31 AM. This article is licensed under a Creative Commons Attribution-NonCommercial 3.0 Unported Licence.

present in the aqueous matrix. The amount of Pb^{2+} uptake from the yeast biomass was calculated using eqn (1):

$$q_t = \frac{V}{m}(c_0 - c_t) \quad (1)$$

where q_t is the Pb^{2+} mass (μg) adsorbed per gram of yeast biomass after t contact time (μg g^{-1}); c_0 is the initial Pb^{2+} concentration in the aqueous solution (μg L^{-1} or ppb); c_t is the residual Pb^{2+} concentration measured after t contact time (μg L^{-1} or ppb); m is the dry weight of yeast biomass in the solution (g), and V is the volume of the aqueous solution (L). If equilibrium has been reached and c_t is c_e, then q_t is q_e.

Equilibrium isotherm data are obtained as the q values measured after 1 d of contact of yeast biomass (m: 0.005 g) with aqueous solutions (0.2 L) of different initial Pb^{2+} concentrations (c_0: 20, 40, 100, 200, 300, 500, 700 and 1000 ppb), respectively. ESI 1.6† describes the fitting of first-principles derived curves to kinetics data recorded at periodic intervals (*i.e.*, 0 min, 5 min, 15 min, 30 min, 1 h, 2 h, 4 h, 8 h, 24 h) of contact with yeast biomass (m: 0.005 g) in aqueous solutions (0.2 L) with c_0 of 100 ppb.

2.8 Confocal imaging

The Calcofluor White stain, 5 mM in water (Biotium, USA), was used to image yeast cells inside the hydrogel capsules. Calcofluor White is a fluorescent blue dye that binds with cellulose and chitin, and particularly with the bud scars of yeast cells, because of their high chitin concentrations. Yeast staining and imaging protocols were applied as suggested by the manufacturers.

Nile Blue acrylamide (Polysciences, USA) was dissolved to obtain a 0.01 mg ml^{-1} solution in the monomer phase described previously, and polymerized into the hydrogel matrix to visualize it.

Samples stained using Calcfluor White and Nile Blue acrylamide were washed to remove any unbound cells and dye, and imaged using an Olympus FV1000 Multiphoton Laser Scanning Confocal Microscope with a 10× water immersion objective. A 720 nm laser was used to excite both dyes. Calcfluor White emission was measured in 460–500 nm and Nile Blue acrylamide emission was measured in 380–560 nm to account for local solvent variations.

The Leadmium Green AM dye (Invitrogen, Thermo Fischer Scientific, USA) was used to detect and image lead on yeast cells. It is a highly specific indicator that allows for the detection of nanomolar levels of lead in microbial cells. The reagent preparation, staining and imaging protocols were applied as suggested by the manufacturer.

Samples stained with Leadmium Green AM dye were imaged using a Zeiss LSM 980 with Airyscan 2 Laser Scanning Confocal Microscope with a 10× air objective and a 488 nm laser for excitation. Fluorescence was measured at 520 nm and longer wavelengths.

2.9 Mechanical characterization of yeast-laden capsules

The hydrogel-laden capsules (D ~500 μm) were mechanically characterized in unconfined compression in deionized (DI) water. Prior to the tests, all samples were stored in DI water, at 4 °C. The Mach-1 v500c system (Biomomentum, Laval, Canada) equipped with a flat punch and a 10 N uniaxial load cell was used for the compression experiments. The experimental setup and a video of the experiments are shown in Fig. S4 and Movie S1.† The tests were performed in displacement-controlled conditions with a rate of 0.4 mm s^{-1}. The load–displacement data were collected and the average properties for six capsules are reported here.

The compressive behavior of spherical hydrogel capsules is non-trivial due to a continuously increasing surface area of contact between the specimen and the testing punch during compression. Hertz solved this contact problem for linearly elastic materials, predicting that the force exerted by a spherical body under small deformation (%) can be expressed as:[35,36]

$$P(r) = \frac{16GR_0^{1/2}}{3}\left[R_0 - \frac{r}{2}\right]^{3/2} \quad (2)$$

where, $P(r)$ is the force (equal to the load in Fig. 4) exerted by the specimen when the distance separating the surface of the compressing plate from the bottom of the solvent bath (Fig. S4†) is r ($r < 2R_0$), G is the shear modulus and R_0 is the initial radius of the hydrogel capsule. The elastic modulus, E, can be obtained by:

$$E = 2G(1 + n) \quad (3)$$

where, n is the Poisson's ratio and was assumed to be 0.5 for such hydrogel materials.[37] Finally, the force $P(r)$ is:

$$P(r) = EA_{\text{Hertz}} \quad (4)$$

where, A_{Hertz} is as an effective area given by:

$$A_{\text{Hertz}}(r) = \frac{8R_0^{1/2}}{3(1+n)}\left[R_0 - \frac{r}{2}\right]^{3/2} \quad (5)$$

The data in Fig. 4b and c are obtained in the initial range of 10% amplitude of the sample height, a regime in which Hertzian contact mechanics offers accurate predictions. The estimated effective elastic modulus, E, was 6.28 ± 0.63 MPa, as fitted using eqn (4). The maximum load before failure, $P_{\max}$ was at 0.88 ± 0.04 N, while the amplitude at which all samples burst was at 80% of the total sample height.

2.10 Biofilter design, operation, and characterization

The biofilter is constructed by packing a 3 ml BD syringe (inner diameter 8.66 mm) with 1.6 g yeast-laden hydrogel capsules. Both ends are closed with syringe filters that serve as frits to contain the capsules, and water is flown through to increase packing within the biofilter. The length of the packed portion is measured to be 4.2 cm, yielding a superficial packed volume of 2.47 ml. The packing fraction is 0.65, and the biofilter contains ~24 600 capsules.

Contaminated water containing lead at a concentration of 100 ppb is injected through the packed bed biofilter at a flow rate of 0.1 ml min^{-1} using a syringe pump. The flow rate is set so that the residence time/contact time (8.45 min) is similar to the contact time in typical water treatment facilities (~10 min), while

Open Access Article. Published on 15 May 2024. Downloaded on 2/18/2026 8:24:31 AM.
This article is licensed under a Creative Commons Attribution-NonCommercial 3.0 Unported Licence.

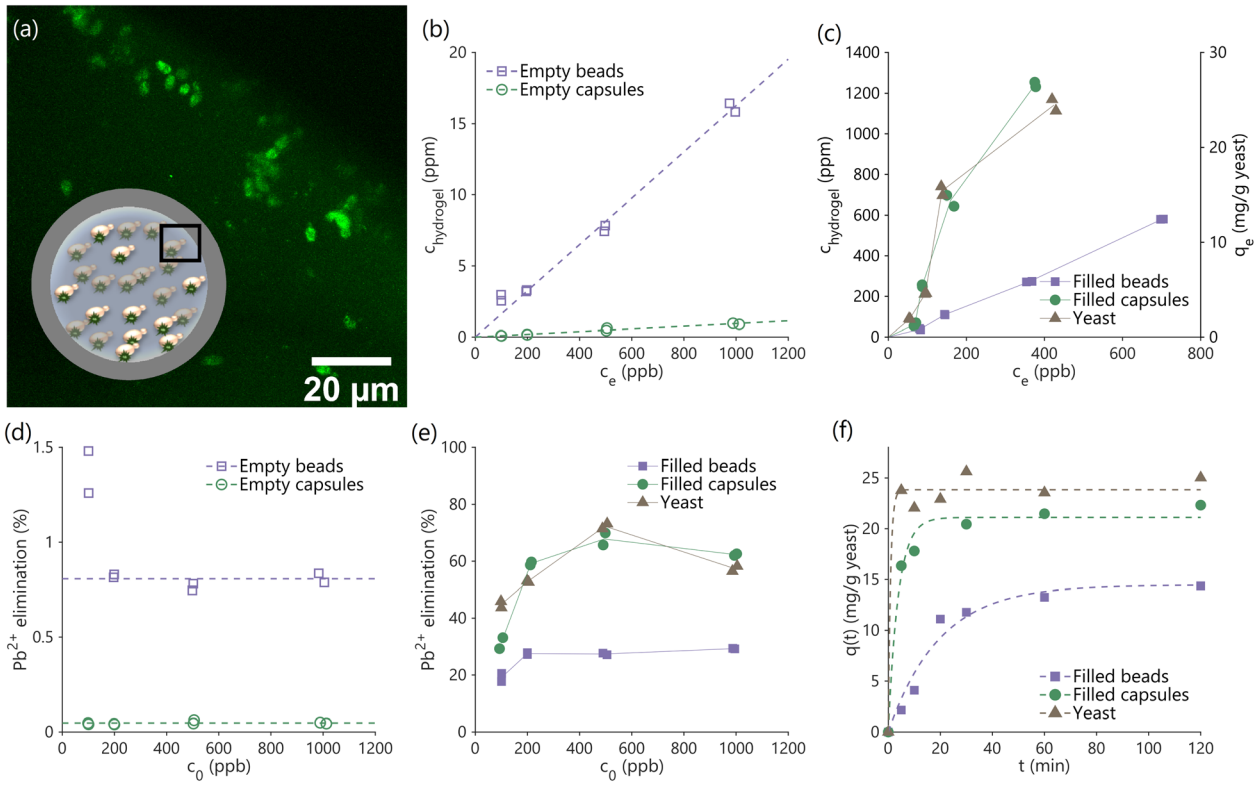

Fig. 3 Uptake of lead by yeast-laden hydrogels. (a) The interior of a hydrogel capsule used to absorb lead, visualized using confocal fluorescence microscopy after Leadmium Green AM staining to show lead. The image captures a cross-section near the capsule wall, as indicated in the inset. (b) Equilibrium absorption isotherms showing the concentration of lead inside the hydrogel against that in the supernatant for blank hydrogel beads and capsules without yeast. (c) The same equilibrium adsorption isotherms when using yeast-laden hydrogel capsules and beads, compared with those for free yeast in water. Lines connect the midpoints of experimental replicates. (d and e) Percentage elimination of lead by (d) blank capsules and beads, and (e) yeast-laden (filled) capsules and beads, and free yeast. Lines connect the midpoints of experimental replicates. (f) The kinetics of lead uptake by free yeast cells, and yeast-laden (filled) beads and capsules, from water with an initial lead concentration (c_0) of 1000 ppb. Error bars in all plots are <±1%.

being at least double the yeast-laden capsule equilibration time (3.83 min, see Fig. 3f).

A FlexiForce piezoelectric force sensor connected to a National Instruments NI myDAQ Student Data Acquisition Device that interfaces with MATLAB Simulink is used to measure the pressure drop across the biofilter. First, the force exerted by the syringe pump on the syringe to flow water through the biofilter at the desired flow rate is measured. Then, the biofilter (including the syringe filters on either end) are removed to obtain the force contribution attributable to the remainder of the setup, and this contribution is subtracted to obtain the force needed to pump water through the biofilter. Using a similar approach, the contribution of each filter component may be obtained and accounted for. Finally, we obtain the relevant force requirement to be 178 gram-force or 1.7462 N, and the pressure drop across the packed portion of the biofilter as 29.646 kPa.

3 Results and discussion

3.1 Synthesis of yeast-laden hydrogel capsules

Saccharomyces cerevisiae (*S. cerevisiae*) yeast cells were cultured, harvested, lyophilized (freeze-dried) and converted to powder, as described in Materials and methods.[1] We explored two encapsulation strategies to increase the effective size of the yeast while retaining functionality, preparing hydrogel beads (solid particles in which yeast are embedded) and capsules (hydrogel shells containing void space filled with water and yeast). Mass transport limitations and hydrogel–yeast interactions were expected to be significantly different due to changes in geometry, as were the mechanical properties. Comparing the performance of yeast-laden beads to capsules enabled us to better understand the effect of the hydrogel encapsulation on the properties of yeast, and optimize a proposed scaled up process.

Yeast-laden hydrogel beads and capsules are synthesized using an off-the-shelf microfluidic device ('micro-cross', Fig. 2a). We start by preparing a monomer solution (light blue in Fig. 2a) containing PEGDA monomers dissolved in water. Lyophilized yeast powder (Fig. 2b) is suspended in the monomer solution using a small amount of surfactant (0.05% (w/w)) to stabilize the suspension. The monomer solution is processed in the microfluidics setup (Fig. 2a and S1†) to obtain monodisperse droplets by pinch-off. An extensive preconditioning of the setup and stabilization of the monomer solution enables us to achieve significantly higher yeast loadings inside the

© 2024 The Author(s). Published by the Royal Society of Chemistry

Open Access Article. Published on 15 May 2024. Downloaded on 2/18/2026 8:24:31 AM. This article is licensed under a Creative Commons Attribution-NonCommercial 3.0 Unported Licence.

hydrogels compared to prior work (see Materials and methods), eliminating challenges associated with yeast cells blocking the micro-cross pores.[34] A photoinitiator (PI) triggers the free-radical chain growth polymerization of the PEGDA dissolved in monomer droplets upon exposure to UV light, crosslinking the monomer into a solid gel. The photoinitiator may be dissolved either in (i) the monomer solution or in (ii) the oil phase (light yellow in Fig. 2a), to obtain either beads or capsules respectively.

In the first case, when the photoinitiator is dissolved in the monomer solution, the polymerization occurs in the entire bulk of the monomer-containing droplets, leading to the formation of solid hydrogel beads. In the second case, when the photoinitiator is dissolved in the oil phase, the polymerization begins at the oil-droplet interface where the photoinitiator and the PEGDA monomers are in contact. The reaction then slowly progresses into the interior of the droplets as the photoinitiator molecules slowly dissolve and diffuse from the interface into the monomer solution, leading to the formation of capsules. Since the polymerization reaction rapidly stops after UV exposure is terminated, it is possible to prepare capsules with tunable wall thickness by controlling the duration of the UV exposure. Here, the capsules have a wall thickness that is approximately 30 μm (see ESI 1.5†), which may also be tuned by changing the wavelength and intensity of UV light, the tubing material, and similar parameters.[38,39] Capsules and beads prepared in this manner are washed with DI water to remove unreacted PEGDA and photoinitiator, and any unbound yeast. A picture of yeast-laden capsules prepared using this method is shown in Fig. 2c and S2†.

As shown in Fig. 2b, the diameter of individual yeast cells is approximately 5 μm. The mesh size of the prepared hydrogels was calculated to be 2.09 nm in the absence of yeast cells within the hydrogel matrix, and 2.03 nm if yeast cells are present inside the matrix, using a combination of swelling measurements and Canal-Peppas theory (see ESI 1.1 and 1.2†). Since the size of the yeast cells is much greater than the mesh size of the encapsulating hydrogel (~2,500×), we can guarantee that the yeast cells are permanently trapped within the hydrogel and cannot escape in the water that is to be treated. Such an encapsulation approach, which does not require the creation of chemical bonds between moieties on the yeast surface and the hydrogel matrix is desirable to ensure minimal effects on the properties of the yeast cells. Confocal microscopy images in Fig. S3† indicate that the yeast cells are intact after the polymerization process, allowing effective encapsulation. Fig. S2† shows an unstained hydrogel bead containing stained yeast cells after resting in a water bath overnight. The absence of any stained free yeast cells in the fluid surrounding the bead also demonstrates effective encapsulation.

Fig. 2d and e are confocal microscopy images of the interior of yeast-laden hydrogel beads and capsules, respectively. Yeast cells (cyan) are seen to be uniformly distributed within the hydrogel bead, but not within the hydrogel capsule. The non-uniform distribution of cells within the yeast capsule is a combination of the settling of yeast-cells under the effect of gravity, and the adhesion of yeast cells to the inner surface of the capsule walls (yellow). However, a significant number of yeast cells may nonetheless be seen to be free of the capsule walls and mobile within the capsule. The capsule walls are solid and prevent the escape of yeast cells as previously described.

3.2 Adsorption kinetics and isotherm

We studied the kinetics of and equilibrium uptake of lead(II) ions from water containing a known quantity of lead using hydrogel beads and capsules (see Materials and methods). Kinetics measurements are essential to demonstrate lead removal within the limited contact times in real-world adsorption processes, and necessary to size and design practical filters in combination with equilibrium measurements. All experiments were performed on an equal yeast basis (200 ml lead-contaminated water treated using 5 mg yeast, or 100 mg hydrogel beads/capsules containing 5% (w/w) yeast, or 95 mg of hydrogel beads/capsules not containing yeast as controls), at pH 5.0 at which dissolved lead primarily exists as lead(II) ions. The liquid supernatant containing dissolved lead and solid hydrogel phases were separated by gravitational settling, and the supernatant was analyzed to measure residual lead concentrations. A mass balance approach was used to calculate lead concentrations inside the capsules, beads and yeast at equilibrium.

Yeast-laden hydrogel capsules after biosorption were stained with Leadmium Green AM to visualize lead within the capsules using confocal fluorescence microscopy. The acquired images clearly show lead bound on the encapsulated yeast cells (Fig. 3a), while the background hydrogel matrix is only weakly fluorescent, indicating the uptake of lead by the capsules, and that the majority of lead uptake is due to the yeast cells and not the hydrogel matrix.

Performing equilibrium experiments at varying initial lead concentrations (c_0: 100–1000 ppb) allows us to construct isotherms (Fig. 3b and c) that can guide the design of larger scale filters. Fig. 3b shows the concentration of lead in the interior of empty hydrogel capsules and beads ($c_{hydrogel}$) against the concentration in the supernatant at equilibrium (c_e). The data fit linear isotherms, as can be expected based on prior work that used hydrogels for water treatment[30] and described in ESI 1.3.† Lead ions are seen to weakly partition into the hydrogels, which may be attributed to a combination of hydrogen bonding between the PEGDA hydrogel and water associated to the lead ions, and to weak van der Waals forces. The empty hydrogel beads were also seen to have a significantly higher internal concentration of lead than the empty capsules, and this difference can be attributed to the greater quantity of polymerized PEGDA to bind lead within the beads compared to the capsules (see ESI 1.3†).

The yeast-laden hydrogel beads and capsules have significantly higher affinity to lead ions compared to yeast-free blanks, as can be seen by comparing the magnitudes of data on the second y-axis of Fig. 3c to the data in Fig. 3b (also see Fig. 3d and e). The isotherms in Fig. 3c, shown for free yeast as well as yeast-laden hydrogel beads and capsules, indicate significant lead binding by yeast in all three cases (~2% of the total mass of the yeast). Importantly, trapping yeast cells inside hydrogel

Open Access Article. Published on 15 May 2024. Downloaded on 2/18/2026 8:24:31 AM. This article is licensed under a Creative Commons Attribution-NonCommercial 3.0 Unported Licence.

capsules does not significantly affect their ability to bind with lead (only a ~10% loss in capacity; c_0 = 1000 ppb), while immobilization within hydrogel beads significantly reduces binding capacity (~40% loss in capacity; c_0 = 1000 ppb). This reduction in uptake capacity may be due to: (1) interactions between the hydrogel matrix and the yeast cell wall, outcompeting interactions between the functional groups present on yeast cell wall which are responsible for binding lead ions,[1] or (2) the effect of the photoinitiator on yeast properties. Photoinitiators form free radicals when exposed to UV light, thereby triggering polymerization reactions. However, the same free radicals may also attack the yeast cells, damaging chemical moieties responsible for binding lead.[40] Since hydrogel beads have a greater quantity of hydrogel matrix surrounding yeast cells (see ESI 1.4†) and are prepared by dissolving the photoinitiator in the same phase as the yeast cells (as opposed to capsules), both these effects which limit lead uptake may be expected to be more significant in beads than capsules, leading to the reduced capacity of beads compared to capsules seen in Fig. 3c.

The adsorption isotherms of yeast and yeast-laden capsules are not linear and seem to follow Langmuir's isotherm model (Fig. 3c).[41] A similar effect was observed in prior work that used free yeast to bind lead.[1] A non-linear shape is also apparent from the presence of a sharp peak in the plot of lead elimination against initial concentration (Fig. 3e; unlike the flat profiles from linear isotherms in Fig. 3d), a feature of Langmuir adsorption model, borrowed from the ideal adsorption theory of gases. The presence of a peak indicates the existence of an optimal initial lead concentration for water treatment in batch operations, but does not affect the design of continuous flow-through filters. If a linear isotherm is nevertheless fit to the data in Fig. 3c as a first-order approximation, we obtain a partition coefficient (ratio of internal to external concentration at equilibrium ($(c_{hydrogel}/c_e)$), obtained as the isotherm slope) of ~3000, which is much greater than those observed in hydrogels optimized for water treatment in prior work,[30] indicating the superior binding of functional groups on yeast cells compared to traditional chelating agents and other synthetic moieties used to bind lead in these hydrogels. Interestingly, unlike yeast-laden capsules, yeast-laden hydrogel beads also have nearly linear isotherms, which may be explained by a combination of reduced capacity (ESI 1.3†), and greater binding of lead to the hydrogel matrix as a fraction of binding to the yeast cells.

Contact times in real-world adsorption processes for water treatment are limited (~10 min),[22,23] making it important to assess the rate of lead removal by free yeast and yeast-laden hydrogel beads and capsules. Fig. 3f shows the amount of adsorbed lead over time starting with an initial lead ion concentration, c_0, of 1000 ppb. This kinetics data may be fit to an analytical expression based on first-order kinetics to obtain mass transfer rates that can guide the design of filters at scale (ESI 1.6 and 1.7†). The use of the first-order kinetics model has been previously validated in studies that separately examined the use of free yeast and pure hydrogels for lead uptake.[1] Regression also yields time constants for the uptake process (0.88 min for free yeast, 3.83 min for yeast-laden capsules, and 19.57 min for yeast-laden beads). The removal of lead can be seen to be most rapid using free yeast, followed by yeast-laden capsules, and finally yeast-laden beads. These trends may be expected due to the increasing restrictions on yeast mobility and mixing as we shift from free yeast in water, to yeast in hollow hydrogel capsules, and finally to yeast completely immobilized inside solid hydrogel beads. The equilibrium time constants for yeast-laden capsules are significantly shorter than the 10 min contact times in real-world adsorption processes, which, combined with their high capacity for binding lead (>20 mg per g yeast) (Fig. 3c and e), makes them advantageous for large-scale application, such as in bioreactors for filtration.

3.3 Mechanical characterization and proof-of concept biofilter

Bioreactor beds, during their operational cycles, are subject to fluid dynamics-induced stresses as well as varying internal pressures.[42] Without a basic understanding of the yeast-laden hydrogel capsules' mechanical properties, these packed beds can fail, compromising the effectiveness of the biosorption process. Furthermore, understanding capsule deformation under operational conditions is vital. Even minor deformations can significantly alter flow dynamics, which, in turn, can adversely affect lead adsorption. Indeed, compressed bioreactor beds can exhibit increased pressure drop, reduced flow rates, or channeling, with flow bypassing certain bed regions and resulting in insufficient pollutant removal.[43] Here, as a first step towards scale up, we performed mechanical testing to assess the robustness of the yeast-laden hydrogel capsules and to guide the design of a cm scale, packed-bed bioreactor operated as a flow-through filter (biofilter) as a proof-of-concept of our approach.

We evaluated the effective elastic modulus (E) of the yeast-laden hydrogel capsules, and the maximum compressive load (P_{max}) they can withstand before failure (bursting of the capsules). To achieve loading conditions similar to those during biofilter operation, we performed uniaxial, displacement-controlled, compression tests of the capsules in water, as shown in Fig. 4a (experimental details in ESI 1.8†). The compression tests showed a non-linear dependence between load (P) and displacement of the compressing punch (δ) (green data points in Fig. 4b). The load–displacement data can be fitted as $P \propto \delta^{3/2}$ (black dashed line in Fig. 4b). Such a dependence is common in homogenous, isotropic, linear, elastic materials, such as cross-linked, synthetic hydrogels,[44–46] tested under small deformations and quasi-static loading conditions, and can be described by the Hertzian model.[35,36] Although the yeast-laden hydrogel capsules are not typical homogenous hydrogel materials, since their interior is hollow and contains yeast cells (Fig. 2e), E can still be approximated using the Hertzian model, given the observed, non-linear $P \propto \delta^{3/2}$ dependence. By fitting the experimental data, while assuming a Poisson ratio (n) of 0.5, which is typical for such materials,[37] we obtain $E = 6.28 \pm 0.63$ MPa (Fig. 4c). The P_{max} that the capsules can withstand without bursting is about 0.88 ± 0.04 N. The Hertzian model is

 © 2024 The Author(s). Published by the Royal Society of Chemistry

Open Access Article. Published on 15 May 2024. Downloaded on 2/18/2026 8:24:31 AM.
This article is licensed under a Creative Commons Attribution-NonCommercial 3.0 Unported Licence.

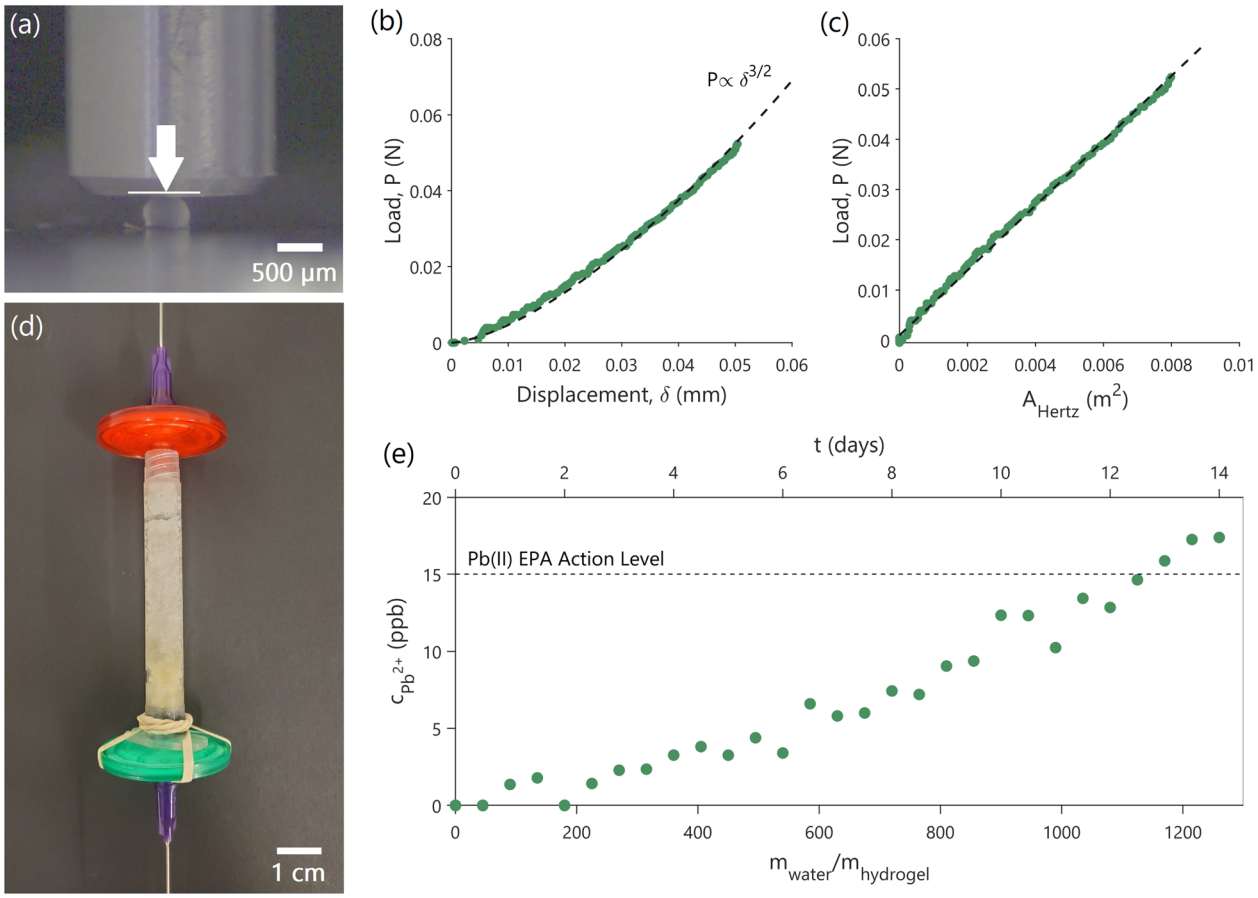

Fig. 4 Mechanical testing of capsules and proof-of-concept biofilter. (a) Experimental setup showing uniaxial, displacement-controlled, compression tests of the hydrogel capsules in water. The metallic punch is used to compress the hydrogel capsule in the indicated direction (white arrow) while the load and the applied displacement are measured. (b) Load *versus* displacement experimental data show a $P \propto \delta^{3/2}$ dependence. (c) Fitting of the experimental data using the Hertzian model provides an effective elastic modulus (E) of 6.28 ± 0.63 MPa. A_{Hertz} is the effective capsule area, described in eqn (5). (d and e) The proof-of-concept cm-scale biofilter (d) containing yeast-laden hydrogel capsules constructed for this study, and the breakthrough curve (e) showing the concentration of lead in treated water coming out ($c_{Pb^{2+}}$) as a function of time of operation and amount of water cleaned. Reported concentrations are ± 0.7%. The initial concentration of incoming water is 100 ppb. The dashed line shows the USEPA action level for lead.

used here to get a first approximation of E. In future efforts, E can be determined in a more accurate manner by solving the boundary element problem.[47]

As a proof-of-concept of the scalability of our approach, 1.6 g (or about 24 600 capsules) of yeast-laden hydrogel capsules were packed in an empty syringe to prepare a simple biofilter (Fig. 4d), through which lead contaminated water can be continuously pumped through to treat it. The filter is operated to have a contact time of 8.45 min, which is representative of contact times in real-world adsorption-based water-treatment processes.[22,23] Considering the operational parameters and capsule dimensions, we estimated a developed drag force (F_{drag}) of ~0.8 μN and a maximum stress (σ) of ~4.00 Pa on each yeast-laden hydrogel capsule (ESI 1.8†). Given the mechanical behavior of the capsules, $E = 6.28 \pm 0.63$ MPa and $P_{max} = 0.88 \pm 0.04$ N, there remains a substantial elastic range before approaching the failure limits of the capsules. As a result, it is highly unlikely that the capsules would undergo significant deformation or encounter structural failure within the biofilter, ensuring that they will retain their functionality throughout biofilter operation.

Indeed, the filter was continuously operated for a period of 14 days, cleaning water with an initial lead concentration of 100 ppb, during which period we did not observe any bursting of capsules. Fig. 4e shows the concentration of lead ($c_{Pb^{2+}}$) in water after treatment using our biofilter as a function of time and the cumulative amount of water treated relative to the mass of the hydrogel capsules ($m_{water}/m_{hydrogel}$). The 1.6 g biofilter is able to treat over 1.5 L of contaminated water to below the USEPA lead action level for a period of 12 days before it needs to be replaced. Increasing the mass of hydrogel capsules within the filter will increase filter lifetime, which is governed by the equilibrium isotherms and kinetics shown in Fig. 3, as described in ESI 1.7.†

The maximum water flow rate through the biofilter (Q_{max}) is limited by capsule failure due to pressure, and estimated using mechanical data (ESI 1.8†) to be 1.87 L s^{-1} or ~160 m^3 per day. To put this into perspective, the standard flow rate for a US household kitchen faucet is 0.18 L s^{-1}.[48] This indicates that our

Open Access Article. Published on 15 May 2024. Downloaded on 2/18/2026 8:24:31 AM. This article is licensed under a Creative Commons Attribution-NonCommercial 3.0 Unported Licence.

biofilter approach can be effectively scaled for use in household settings without compromising the capsules' structural integrity and performance. Furthermore, the derived Q_{max} aligns with the average wastewater flow rate of a municipal treatment plant that caters to a small community of roughly 400 residents.[49] As such, our current biofilter approach could be scaled to accommodate communities of up to a few hundred individuals. Modifications in the yeast-laden hydrogel capsules' geometry, such as size and wall thickness, and adjustments in the hydrogel material properties can be implemented to meet the requirements of larger populations ($\geq$400 people).

4 Conclusions

This study presents a technology for the scale up of yeast biosorption to remove trace lead from water without requiring additional treatment steps to remove yeast. Experimental data show that the developed hydrogel capsules have consistent composition, controlled size, high porosity and hydrophilicity, and can effectively retain the yeast cells without diminishing their lead uptake capacity. The yeast-laden capsules exhibit an uptake capacity of 21 mg g^{-1}, while free yeast achieve 23 mg g^{-1} under the same conditions ($c_0 = 1000$ ppb), a loss in capacity of only ~10%. Equilibrium is rapidly attained within 5 min of contact, allowing the use of yeast-laden hydrogel capsules in real-world adsorption processes for water treatment, which have contact times of about 10 min. Furthermore, our capsule approach outperforms solid hydrogel beads, offering a 50% increase in effectiveness (with equilibrium uptake capacities of 21 mg g^{-1} and 14 mg g^{-1}, respectively; $c_0 = 1000$ ppb). The yeast-laden hydrogel capsules also demonstrate mechanical robustness, and are not susceptible to bursting or significant compression under normal operating conditions. These results, combined with the effective performance of a proof-of-concept biofilter that cleaned contaminated water ($c_0 = 100$ ppb) to within the USEPA drinking water guidelines for 12 days, suggest that our method is suitable for direct scaling-up and implementation in household settings, such as kitchen faucets, or in small treatment plants that accommodate communities of up to a few hundred individuals.

Previous attempts to scale-up biosorption using immobilized microbial cells have failed mostly due to chemical alterations of cell structures caused by immobilization agents, lack of mechanical robustness, and unfavorable solute mass transfer rates.[21] In contrast, our approach successfully addresses these challenges, enabling yeast to perform nearly as effectively as in its free state while encapsulated. This achievement is primarily attributed to the minimal interaction between the carrier (PEGDA) and the biosorbent, (inactive, lyophilized yeast biomass), and the protection of yeast from chemical alteration. Such minimal interference represents a significant success of our work and is a critical step towards the scalability and commercialization of the proposed approach. Additional engineering experiments can enable the scale-up of this approach for larger industrial or municipal settings. Potential modifications in the yeast-laden hydrogel capsules' geometry, and adjustments in hydrogel's material properties can be explored to ensure structural and functional integrity under varying operational conditions and in unforeseen situations, such as abrupt changes in pressure, temperature, or flow rates. Additionally, conducting a techno-economic analysis to evaluate the commercial competitiveness of the scaled-up approach is essential for translating these findings into the market.

Substantial quantities of residual or surplus yeast are generated from fermentation industries, with over 50 000 tons annually produced from beer production in the US alone.[27,50] This is an extremely underutilized, low-value or even negative-value resource, not suitable as a human dietary supplement due to high levels of nucleic acids.[27] In parallel, PEGDA is an inexpensive, non-toxic, easy-to-make hydrogel,[51] which can also be renewably sourced, as poly(ethylene) glycol (PEG) can be derived from bio-based sources, such as plant-based feedstocks.[52,53] Combining these low-cost, easy-to-mass-produce materials can result in environmentally-friendly, locally sourced water treatment methods. The circular economy principles inherent in this approach not only reduce waste and environmental impact compared to conventional water treatment approaches, such as RO, but also create economic opportunities within the communities where these resources are available. Therefore, this approach has the potential to address environmental equity challenges, particularly in low-income areas and communities of color that have historically faced environmental pollution and limited access to clean water.[54]

Author contributions

D. G., P. M. S., and C. E. A. conceived the study, and designed and performed the experiments. P. S. D. provided technical inputs. All authors analyzed the data and contributed to discussions and writing.

Conflicts of interest

There are no conflicts to declare.

Acknowledgements

D. G. was supported by the Rasikbhai L. Meswani Fellowship for Water Solutions and the MIT Abdul Latif Jameel Water and Food Systems Lab (J-WAFS). P. M. S. was supported by funding from the Renewable Bioproducts Institute at Georgia Tech for performing experiments and is thankful to Prof. C. Meredith. P. M. S. thanks the Molecular Evolution Core (Dr S. Biliya and Dr N. Djeddar) and the Biomolecular Analysis Core Facilities (Dr B. Yang) at the Parker H. Petit Institute for Bioengineering and Bioscience at Georgia Tech for providing access to their equipment for the cultivation and preparation of yeast cells. D. G. and P. M. S. also thank the MIT Center for Environmental Health Sciences (CEHS) and Dr B. Fedeles for supporting ICP-MS analyses of samples. D. G. also thanks J. Wyckoff and I. Yadav for supporting confocal imaging of samples. P. M. S. is grateful to Prof. Neil Gershenfeld from the MIT Center for Bits and Atoms for the fruitful initial discussions regarding the scalability of this approach and support of initial research endeavors.

© 2024 The Author(s). Published by the Royal Society of Chemistry

Open Access Article. Published on 15 May 2024. Downloaded on 2/18/2026 8:24:31 AM. This article is licensed under a Creative Commons Attribution-NonCommercial 3.0 Unported Licence.

References

1 P. M. Stathatou, C. E. Athanasiou, M. Tsezos, J. W. Goss, L. C. Blackburn, F. Tourlomousis, A. Mershin, B. W. Sheldon, N. P. Padture, E. M. Darling and H. Gao, *Commun. Earth Environ.*, 2022, **3**(1), 132.

2 J. S. Casas and J. Sordo, *Lead: Chemistry, Analytical Aspects, Environmental Impact and Health Effects*, Elsevier, 2006.

3 Aquasana, Health Effects of Lead in Drinking Water, 2023, **https://www.aquasana.com/info/health-effects-lead-in-drinking-water-pd.html**, Accessed: 2023-10-17.

4 USEPA, Basic Information about Lead Air Pollution, 2023, **https://www.epa.gov/lead-air-pollution/basic-information-about-lead-air-pollution**, Accessed: 2023-12-11.

5 USEPA, Basic Information about Lead in Drinking Water, 2023, **https://www.epa.gov/ground-water-and-drinking-water/basic-information-about-lead-drinking-water**, Accessed: 2023-12-11.

6 B. P. Lanphear, S. Rauch, P. Auinger, R. W. Allen and R. W. Hornung, *Lancet Public Health*, 2018, **3**(4), e177–e184.

7 CDC, 2022-2023 U.S. Flu Season: Preliminary In-Season Burden Estimates, 2023, **https://www.cdc.gov/flu/about/burden/preliminary-in-season-estimates.htm**, Accessed: 2023-12-11.

8 Aquasana, U.S. Cities with High Levels of Lead in Drinking Water, 2023, **https://www.aquasana.com/info/us-cities-with-high-lead-levels-pd.html**, Accessed: 2023-10-17.

9 R. J. Santucci Jr and J. R. Scully, *Proc. Natl. Acad. Sci.*, 2020, **117**(38), 23211–23218.

10 Reuters, The thousands of U.S. locales where lead poisoning is worse than in Flint, 2016, **https://www.reuters.com/investigates/special-report/usa-lead-testing/**, Accessed: 2023-12-11.

11 USEPA, Lead and Copper Rule, 2023, **https://www.epa.gov/dwreginfo/lead-and-copper-rule**, Accessed: 2023-10-17.

12 USEPA, Understanding the Lead and Copper Rule, 2019, **https://www.epa.gov/sites/default/files/2019-10/documents/lcr101_factsheet_10.9.19.final_.2.pdf**, Accessed: 2023-10-17.

13 Harvard, EPA's Lead and Copper Rule: Examining Challenges and Prospects, 2021, **https://eelp.law.harvard.edu/2021/01/lead-and-copper-rule/**, Accessed: 2023-10-17.

14 The Guardian, We sampled tap water across the US – and found arsenic, lead and toxic chemicals, 2021, **https://www.theguardian.com/us-news/2021/mar/31/americas-tap-water-samples-forever-chemicals**, Accessed: 2023-10-17.

15 CRC Reports - Tap Water Testing by Location, 2021, **https://uploads.guim.co.uk/2021/04/02/Consumer_Reports_Tap_Water_Test_Results_April_2021_(7).pdf**, Accessed: 2023-10-17.

16 H. Tian, M. A. Alkhadra, K. M. Conforti and M. Z. Bazant, *ACS EST Water*, 2021, **1**(10), 2269–2274.

17 Forbes, How Much Does A Reverse Osmosis System Cost?, 2023, **https://www.forbes.com/home-improvement/home/reverse-osmosis-system-cost/**, Accessed: 2023-10-17.

18 USEPA, Point-of-Use Reverse Osmosis Systems, 2023, **https://www.epa.gov/watersense/point-use-reverse-osmosis-systems**, 2023, Accessed: 2023-12-11.

19 IFI TWG - AHSA-004 - Default Energy Intensity Factors for Water Supply Systems, 2020, **https://unfccc.int/sites/default/files/resource/AHSA-004_DefaultEnergyIntensityFactorsforWaterSupplySystems_v1.pdf**, Accessed: 2023-12-11.

20 U. Ghimire, G. Sarpong and V. G. Gude, *ACS Omega*, 2021, **6**(18), 11794–11803.

21 M. Tsezos, Biosorption: A Mechanistic Approach, in *Geobiotechnology I: Metal-Related Issues*, Springer-Verlag, 2014.

22 P. Jin, X. Jin, X. Wang, Y. Feng and X. C. Wang, Biological Activated Carbon Treatment Process for Advanced Water and Wastewater Treatment, in *Biomass Now - Cultivation and Utilization*, IntechOpen, 2013.

23 Lenntech, Activated Carbon Filters, 2023, **https://www.lenntech.com/systems/deep/activated-carbon/gacfilter.htm**, Accessed: 2023-09-01.

24 G. L. Sun, E. E. Reynolds and A. M. Belcher, *Nat. Sustain.*, 2020, **3**(4), 303–311.

25 J. Wang and C. Chen, *Biotechnol. Adv.*, 2006, **24**(5), 427–451.

26 Y. Ojima, S. Kosako, M. Kihara, N. Miyoshi, K. Igarashi and M. Azuma, *Sci. Rep.*, 2019, **9**(1), 225.

27 A. Jaeger, E. K. Arendt, E. Zannini and A. W. Sahin, *Fermentation*, 2020, **6**(4), 123.

28 W. Yin, X. Wang, Y. Liao, L. Ma, J. Qiao, H. Liu, X. Song and Y. Liu, *Front. Bioeng. Biotechnol.*, 2022, **10**, 849542.

29 D. Gokhale, I. Chen and P. S. Doyle, *ACS Appl. Polym. Mater.*, 2022, **4**(1), 746–754.

30 D. Gokhale, A. F. Hamelberg and P. S. Doyle, *Nat. Mater.*, 2024, **2**, 62–71.

31 R. Foudazi, R. Zowada, I. Manas-Zloczower and D. L. Feke, *Langmuir*, 2023, **39**(6), 2092–2111.

32 L. Z. Xin, M. Carenza, I. Kaetsu, M. Kumakura, M. Yoshida and T. Fujimura, *Int. J. Rad. Appl. Instr. C.*, 1992, **40**(6), 579–584.

33 T. Menegatti and P. Znidarsic-Plazl, *Micromachines*, 2019, **10**(12), 867.

34 M. Steinacher, A. Cont, H. Du, A. Persat and E. Amstad, *ACS Appl. Mater. Interfaces*, 2021, **13**(13), 15601–15609.

35 M. A. Gauthier, J. Luo, D. Calvet, C. Ni, X. X. Zhu, M. Garon and M. D. Buschmann, *Polymer*, 2004, **45**, 8201–8210.

36 Q. J. Wang and D. Zhu, Hertz Theory: Contact of Spherical Surfaces, in *Encyclopedia of Tribology*, Springer, Boston, MA, 2013.

37 A. Gandin, Y. Murugesan, V. Torresan, L. Ulliana, A. Citron, P. Contessotto, G. Battilana, T. Panciera, M. Ventre, A. P. Netti and L. Nicola, *Sci. Rep.*, 2021, **11**(1), 22668.

38 K. W. Bong, J. Lee and P. S. Doyle, *Lab Chip*, 2014, **14**, 4680–4687.

39 Sigma-Aldrich, Applications: Free Radical Initiators, **https://www.sigmaaldrich.com/content/dam/sigma-aldrich/docs/Aldrich/General_Information/photoinitiators.pdf**, Accessed: 2024-03-20.

40 W. Droge, *Physiol. Rev.*, 2002, **82**(1), 47–95.

Open Access Article. Published on 15 May 2024. Downloaded on 2/18/2026 8:24:31 AM.
This article is licensed under a Creative Commons Attribution-NonCommercial 3.0 Unported Licence.

41 I. Langmuir, *J. Am. Chem. Soc.*, 1916, **38**(11), 2221–2295.
42 B. J. Motil, H. K. Nahra and V. Balakotaiah, *SAE Technical Paper*, 2005, 2005–01–3035.
43 M. Balhoff, Modeling the flow of non-Newtonian fluids in packed beds at the pore scale, PhD thesis, Louisiana State University and Agricultural & Mechanical College, 2005.
44 G. Nian, J. Kim, X. Bao and Z. Suo, *Adv. Mater.*, 2022, **34**(50), 2206577.
45 X. Liu, J. Liu, S. Lin and X. Zhao, *Mater. Today*, 2020, **36**, 102–124.
46 K. Kothari, Y. Hu, S. Gupta and A. Elbanna, *J. Appl. Mech.*, 2018, **85**(3), 031008.
47 X. Chen, C. Li and X. X. Wei, *Int. J. Mech. Sci.*, 2016, **118**, 67–76.
48 Aquasana, What is a Typical Home Water Flow Rate?, 2023, **https://www.aquasana.com/info/what-is-a-typical-home-water-flow-rate-pd.html**, Accessed: 2023-12-11.
49 USEPA, About Small Wastewater Systems, 2023, **https://www.epa.gov/small-and-rural-wastewater-systems/about-small-wastewater-systems**, Accessed: 2023-12-11.
50 Brewersassociation.org, National Beer Sales & Production Data, 2022, **https://www.brewersassociation.org/statistics-and-data/national-beer-stats/**, Accessed: 2023-12-11.
51 T. Pelras, S. Glass, T. Scherzer, C. Elsner, A. Schulze and B. Abel, *Polym. J.*, 2017, **9**(12), 639.
52 M. K. Wong, S. S. M. Lock, Y. H. Chan, S. J. Yeoh and I. S. Tan, *Chem. Eng. J.*, 2023, **468**, 143699.
53 Hydrocarbon Processing, Clariant launches 100% biobased surfactants, polyethylene glycols, 2022, **https://www.hydrocarbonprocessing.com/news/2022/02/clariant-launches-100-biobased-surfactants-polyethylene-glycols**, Accessed: 2023-12-11.
54 NRGD, Watered Down Justice, 2019, **https://www.nrdc.org/sites/default/files/watered-down-justice-report.pdf**, Accessed: 2023-12-11.

© 2024 The Author(s). Published by the Royal Society of Chemistry